Research Square

Preprints are preliminary reports that have not undergone peer review.
They should not be considered conclusive, used to inform clinical practice,
or referenced by the media as validated information.

DTYMK Functions as a ceRNA to Promote Glioblastoma Progression and Mesenchymal Phenotype Through miR-7-5p/RAF1/MAPK Signaling

Hao Yuan Wu
Second Affiliated Hospital of Anhui Medical University
Zhi We Wang
Second Affiliated Hospital of Anhui Medical University
Zi Wen Chen
Second Affiliated Hospital of Anhui Medical University
Zhen Xing He
Second Affiliated Hospital of Anhui Medical University
Chen Xi Chang
Second Affiliated Hospital of Anhui Medical University
ZeJin Li
Second Affiliated Hospital of Anhui Medical University
DeRan Zhang
Second Affiliated Hospital of Anhui Medical University
JinRuo Zhang
Second Affiliated Hospital of Anhui Medical University
ZhiHao Yang
Second Affiliated Hospital of Anhui Medical University
Bing Zhao
efy105200@fy.ahmu.edu.cn

Second Affiliated Hospital of Anhui Medical University

Research Article

Keywords: Glioblastoma, DTYMK, mesenchymal subtype, competing endogenous RNA, miR-7-5p, RAF1, MAPK signaling, prognostic model

Posted Date: August 13th, 2026

DOI: https://doi.org/10.21203/rs.3.rs-10603721/v1

License: This work is licensed under a Creative Commons Attribution 4.0 International License.
Read Full License

Additional Declarations:
No competing interests reported.

Table 1 to 3 are available in the Supplementary Files section.

DTYMK Functions as a ceRNA to Promote Glioblastoma Progression and Mesenchymal Phenotype Through miR-7-5p/RAF1/MAPK Signaling

HaoYuan Wu[1+], ZhiWei Wang[1+], ZiWen Chen[1+], ZhenXing He[1], ChenXi Chang[1], ZeJin Li[1], DeRan Zhang[1], JinRuo Zhang[1], ZhiHao Yang[1*] and Bing Zhao[1*]

[1]Department of Neurosurgery, The Second Affiliated Hospital of Anhui Medical University, Hefei 230601, China

***Corresponding authors:**
Professor Bing Zhao and Professor ZhiHao Yang
Department of Neurosurgery, the Second Affiliated Hospital of Anhui Medical University, Anhui Medical University, 678 Fu Rong Road, Hefei, Anhui Province, China 230601.
Email: efy105200@fy.ahmu.edu.cn (Bing Zhao)
efy105422@fy.ahmu.edu.cn (ZhiHao Yang)
[+] These authors have contributed equally to this work and share first authorship.

ABSTRACT

Objective Glioblastoma (GBM) carries a dismal prognosis, and the molecular mechanisms governing its malignant progression remain poorly defined. DTYMK, encoding deoxythymidylate kinase, has been implicated as an oncogenic factor across multiple cancer types, yet its functional role and regulatory mechanism in GBM are unknown. This study aimed to characterize the oncogenic function of DTYMK in GBM, define its contribution to proliferation and mesenchymal (MES) transition, and elucidate the underlying molecular mechanism through which DTYMK exerts its effects.

Methods A six-gene prognostic risk model integrating mitochondrial dysfunction, oxidative stress, and apoptosis-related gene signatures was constructed using LASSO regression and multivariate Cox regression analyses across the Atlas of Cancer Genome (TCGA) and the Chinese Glioma Genome Atlas (CGGA) cohorts. Single-cell transcriptomic profiling was performed to characterize the cellular localization and subtype specificity of DTYMK expression. DTYMK knockdown was conducted in glioma cell lines to evaluate effects on proliferation, apoptosis, invasion, MES transition, and intracellular reactive oxygen species (ROS) levels. In vivo validation employed both subcutaneous and orthotopic intracranial xenograft models. The competing endogenous RNA (ceRNA) mechanism was investigated through bioinformatic prediction, dual-luciferase reporter assays, and rescue experiments using epidermal growth factor (EGF) to reactivate MAPK signaling.

Results The six-gene prognostic model exhibited robust predictive performance in both cohorts, with DTYMK contributing the highest risk coefficient. Single-cell analysis revealed that DTYMK was predominantly enriched in glioma tumor cells, with significant overrepresentation in MES-like subpopulations. DTYMK knockdown suppressed glioma cell proliferation, migration, and invasion, inhibited MES marker expression, and induced apoptosis accompanied by excessive intracellular ROS accumulation. In vivo, DTYMK depletion significantly reduced tumor burden and prolonged survival. Mechanistically, DTYMK functioned as a ceRNA by competitively sequestering miR-7-5p, thereby relieving translational repression of RAF1 and activating the downstream MEK-ERK signaling cascade. EGF-mediated reactivation of the MAPK pathway partially rescued the malignant phenotypes suppressed by DTYMK knockdown, confirming that MAPK activation is the principal effector mechanism of this regulatory axis.

Conclusion This study identifies DTYMK as a key driver of GBM malignancy and MES transition operating through the DTYMK-miR-7-5p-RAF1-MAPK axis, and positions DTYMK as a potential prognostic biomarker and therapeutic target for precision intervention in glioma.

Keywords Glioblastoma, DTYMK, mesenchymal subtype, competing endogenous RNA, miR-7-5p, RAF1, MAPK signaling, prognostic model

Introduction

Gliomas are the most common primary malignant tumors of the central nervous system, arising from glial or glial precursor cells and comprising a broad spectrum of histological and molecular entities with markedly different biological behaviors and clinical outcomes [1]. According to the World Health Organization (WHO) classification, gliomas are defined by integrated histopathological and molecular criteria and range from relatively indolent lower-grade lesions to highly aggressive malignancies [2]. Among them, WHO grade IV glioblastoma (GBM) represents the most lethal primary brain malignancy in adults [3]. Based on analysis of gene expression profiles from the TCGA database, GBMs have been reclassified into four distinct molecular subtypes-namely proneural, neural, classical, and mesenchymal (MES) [4]. Patients with MES GBM exhibit a more aggressive form of the disease, characterized by an elevated propensity for relapse and highly infiltrative growth [5]. This therapeutic dilemma primarily stems from the highly invasive and recurrence-prone nature of GBM, the pathological basis of which lies in the rapid proliferative capacity and MES transition potential of GBM cells [6]. In recent years, the rapid advancement of bioinformatics tools has facilitated the construction of integrated prognostic models capable of accurately predicting patient outcomes and identifying critical disease-driving biomarkers [7]. Hence, clarifying the molecular mechanisms that govern the proliferation and

mesenchymal transformation of GBM holds considerable significance for the discovery of biomarkers with clinical application value and therapeutic targets.

DTYMK catalyzes the phosphorylation of dTMP to dTDP and occupies a pivotal position in thymidylate metabolism and dTTP biosynthesis [8]. By maintaining the dTTP pool required for DNA replication, DTYMK may support the nucleotide demands of rapidly proliferating tumor cells [9]. Recent pan-cancer analyses have reported that DTYMK is broadly dysregulated across multiple malignancies and is associated with unfavorable prognosis in several cancer types [10]. In pancreatic adenocarcinoma, DTYMK participates in cell cycle arrest regulation and is associated with tumor immune infiltration and disease progression [11]. In colorectal cancer, elevated DTYMK expression has been identified as a prognostic biomarker correlated with advanced tumor stage and poor progression-free survival [12]. Furthermore, studies have shown that knocking down DTYMK can inhibit the progression of non-small cell lung cancer in patients [13]; meanwhile, in lung adenocarcinoma, DTYMK expression correlates with tumor progression, immune microenvironment characteristics, and poor prognosis [14]. These findings suggest a potential oncogenic role beyond its canonical metabolic function. Nevertheless, the glioma-specific function of DTYMK and its regulatory mechanisms remain insufficiently understood.

miRNAs are endogenous small non-coding RNAs of approximately 22 nucleotides that regulate gene expression mainly by binding to complementary sequences in target transcripts, leading to mRNA degradation or translational repression [15]. Through this post-transcriptional regulatory mechanism, miRNAs participate in many biological processes, including cell proliferation, differentiation, apoptosis, and tumor progression [16]. The competing endogenous RNA (ceRNA) hypothesis proposes that transcripts sharing common miRNA response elements can compete for binding to the same miRNAs, thereby indirectly regulating each other's expression [17]. Although long non-coding RNAs and circular RNAs are widely recognized as important ceRNA regulators, protein-coding mRNAs can also participate in ceRNA networks through their untranslated regions [18]. For example, PTEN mRNA and its pseudogene PTENP1 regulate tumor-suppressive signaling through shared miRNA-mediated interactions, demonstrating that coding and pseudogene transcripts can engage in biologically meaningful ceRNA crosstalk [19]. Of particular interest, recent work in hepatocellular carcinoma revealed a non-canonical ceRNA function of DTYMK, in which DTYMK competitively binds miR-378a-3p to maintain MAPKAPK2 expression and activate NF-κB signaling, thereby promoting tumor growth [20]. This finding suggests that DTYMK may possess regulatory functions beyond nucleotide metabolism and raises the possibility that similar ceRNA-mediated mechanisms could operate in other malignancies. Yet whether DTYMK functions as a ceRNA in glioma, and which miRNA-target axes it may regulate, remains unknown.

In this study, we integrated mitochondrial, oxidative stress, and apoptosis-related gene signatures to construct a six-gene prognostic risk model and identified DTYMK as the most significant risk contributor. Single-cell transcriptomic analysis revealed that DTYMK was preferentially enriched in malignant cells and MES-like subpopulations. Functional experiments demonstrated that DTYMK depletion suppressed glioma cell proliferation, MES transformation, migration, and invasion, while inducing reactive oxygen species (ROS) accumulation and apoptosis. Mechanistically, we found that DTYMK functions as a ceRNA by competitively binding miR-7-5p, a tumor-suppressive miRNA in glioma, thereby relieving repression of its downstream target RAF1 and activating the MAPK signaling cascade. The DTYMK-miR-7-5p-RAF1-MAPK regulatory axis was validated through bioinformatics prediction, correlation analysis, dual-luciferase reporter assays, and functional experiments. Taken together, our findings elucidate the oncogenic mechanism of DTYMK in glioma, positioning DTYMK as a therapeutic target warranting further investigation.

Materials and Methods

Data Sources and Gene Set Curation

Three independent gene sets representing key biological processes dysregulated in malignancy were systematically compiled from public databases. Mitochondria-related genes were retrieved from Human MitoCarta 3.0 [21], whereas oxidative stress-related and apoptosis-related gene sets were obtained from MSigDB [22]. TCGA glioma RNA-sequencing data and comprehensive clinical metadata were downloaded from the GDC Genomic Data Commons portal. GTEx normal brain tissue data were retrieved from the UCSC Xena platform. The CGGA cohort, comprising 693 samples, served as an independent validation dataset [23].

Differential Expression Analysis and Consensus Clustering

A three-way Venn diagram analysis was performed using the VennDiagram R package to identify genes shared across all three categories-mitochondria, oxidative stress-related, and apoptosis-related-yielding a total of 93 consensus genes. Differential gene expression analysis was subsequently conducted between TCGA glioma samples (n = 667) and GTEx normal brain tissue samples (n = 1124) using the limma package in R. Genes meeting the criteria of $\log_2$fold change > 1 and $P < 0.05$ were designated as significantly upregulated, resulting in 27 candidate genes. These genes were then subjected to unsupervised consensus clustering analysis using the ConsensusClusterPlus R package. The optimal number of clusters was determined by evaluating the consensus cumulative distribution function (CDF) curves.

Prognostic Risk Signature Construction

Univariate Cox regression was first applied to the 27 significantly upregulated consensus genes to identify those with individual associations with overall survival in the TCGA cohort. Genes satisfying the significance threshold of $P < 0.05$ were retained as candidate predictors ($n = 21$). Subsequently, LASSO Cox regression with ten-fold cross-validation was performed on these 21 candidates using the glmnet R package. This regularization strategy imposed L1 shrinkage to penalize less informative variables, effectively reducing feature dimensionality and mitigating multicollinearity among predictors. The non-zero coefficients derived from the LASSO model were then carried forward into multivariate Cox regression analysis. A prognostic model incorporating six genes-CASP8, DTYMK, MAPK8, PLAUR, PRODH, and TP73-was established. The model formula below was used to calculate the risk score of each individual patient :

$$Riskscore = \sum_{i=1}^{n} coef(i) \times exp(i)$$

In the above equation, the terms "coef(i)" and "exp(i)" represent the regression coefficients and gene expressions, respectively. Based on the median risk score, all cases were divided into low-risk and high-risk groups. Larger positive risk scores indicate higher predicted hazard and worse prognosis. Patients in TCGA cohorts were dichotomized at the cohort-specific median risk score into high-risk and low-risk groups. Time-dependent receiver operating characteristic (ROC) analysis using the timeROC R package was employed to evaluate the signature's predictive accuracy at 1-, 3-, and 5-year follow-up timepoints, with area under the ROC curve (AUC) values calculated. To assess external validity and generalizability, the identical preprocessing pipeline, coefficient application procedure, and median cutoff dichotomization procedure were applied to the independent CGGA validation cohort. Multivariate Cox regression was subsequently performed to confirm that the risk score remained an independent prognostic factor after adjustment for established clinical variables including age, sex, WHO grade, IDH mutation status, 1p/19q codeletion status, and MGMT promoter methylation status.

miRNA Target Prediction and ceRNA Network Analysis

Candidate miRNAs targeting DTYMK were systematically identified by performing intersection analysis of predictions from two complementary, well-established bioinformatic databases: TargetScan [24] and miRDB [25]. Only miRNAs predicted by both databases were retained, ensuring high specificity. In parallel, predicted targets of the candidate miRNA, miR-7-5p, were obtained

using the same two databases. Expression correlations between pairs of RNA species, including DTYMK-miR-7-5p, miR-7-5p-RAF1, and DTYMK-RAF1, were evaluated using Spearman rank correlation analysis within the StarBase comprehensive database as well as in independent bulk RNA-sequencing datasets, including TCGA and CGGA cohorts, to support mechanistic inference regarding ceRNA function. Direct physical binding between miR-7-5p and the 3′UTRs of DTYMK and RAF1 was validated through dual-luciferase reporter assays. Regulatory directionality was empirically confirmed through systematic perturbation experiments including miRNA mimic transfection, miRNA inhibitor transfection, DTYMK overexpression, and DTYMK knockdown approaches.

Cell Culture and Maintenance

Human glioma cell lines-U251, SW1088, T98G, LN229, U87, SF126, LN18 and HEB were cultured in DMEM supplemented with 10% fetal bovine serum and 1% penicillin-streptomycin antibiotic solution at 37°C under 5% CO_2 in a humidified incubator. Cells were passaged at approximately 70-80% confluence to maintain exponential growth phase and were utilized for experiments within 10-20 passages to minimize genetic drift and phenotypic changes. All cell lines were routinely screened for mycoplasma contamination using the MycoAlert Mycoplasma Detection Kit following the manufacturer's protocol and were authenticated by short tandem repeat (STR) profiling through a certified laboratory.

Transient Transfection with siRNAs and miRNA Mimics

U251 and LN18 glioma cells at 60-70% confluence were transfected with either 50 nM siRNA oligonucleotides targeting DTYMK using Lipofectamine 3000 reagent according to the manufacturer's instructions, or 50 nM miR-7-5p mimic or miR-7-5p inhibitor oligonucleotides using Lipofectamine RNAiMAX. Scrambled oligonucleotide sequences of identical length and GC content served as negative controls in all transfection experiments. Transfection efficiency and expression changes were assessed by quantitative reverse transcription PCR and Western blotting at 24-48 hours post-transfection. Functional assays, including cell viability, migration, invasion, apoptosis, and ROS measurement, were performed at 24-72 hours post-transfection to allow sufficient time for mRNA/protein turnover and phenotypic manifestation.

Generation of Stable DTYMK-Knockdown Cell Lines

To establish cell lines with sustained DTYMK depletion for in vivo xenograft studies, lentiviral short hairpin RNA (shRNA) expression vectors targeting DTYMK were prepared using standard molecular biology techniques. GL261 and LN18 parental glioma cells were transduced with lentiviral particles expressing DTYMK-targeting shRNA under biosafety level 2 containment

conditions. Following transduction, stable cell populations were enriched through puromycin antibiotic selection (2 μg/mL) for two consecutive weeks. Successful and sustained DTYMK knockdown was confirmed by qRT-PCR and Western blotting, and was maintained through continuous culture in medium containing 1 μg/mL puromycin during all subsequent experiments and passages.

Quantitative Reverse Transcription PCR (qRT-PCR)

Total cellular RNA was extracted from cultured cells and tissue samples using TRIzol reagent according to standard protocols. Complementary DNA (cDNA) synthesis employed either standard M-MLV reverse transcriptase kits for mRNA or specialized stem-loop reverse transcription kits for miRNA detection, as stem-loop primers provide superior specificity and sensitivity for mature miRNA quantification. qRT-PCR was performed on a Bio-Rad CFX96 real-time PCR system using SYBR Green chemistry with gene-specific primers. GAPDH served as the endogenous reference gene for normalization of mRNA expression, while U6 normalized miRNA expression to account for variations in RNA extraction efficiency and cDNA synthesis. Relative expression levels were calculated using the comparative 2^-ΔΔCt method.The complete PCR sequence can be found in Table 1 attached.

Western Blot Analysis

Cells and tissue samples were lysed in ice-cold RIPA buffer supplemented with protease inhibitor cocktail and phosphatase inhibitor cocktail to prevent protein degradation and dephosphorylation. Protein concentration was quantified using a BCA protein assay kit . Equal amounts of protein were separated by sodium dodecyl sulfate-polyacrylamide gel electrophoresis (SDS-PAGE) on 10% or 12% polyacrylamide gels and subsequently transferred to polyvinylidene difluoride (PVDF) membranes at 200 V for 1 hour. Membranes were incubated with primary antibodies diluted in 5% non-fat milk in TBST overnight at 4°C. HRP-conjugated anti-mouse or anti-rabbit secondary antibodies were applied for 1 hour at room temperature. The detailed information of all the antibodies we used can be found in Table 2.

Immunohistochemistry (IHC) Analysis

Formalin-fixed, paraffin-embedded tissue section from patient glioma samples and xenograft tumors were deparaffinized in xylene and rehydrated through a graded ethanol series. Antigen retrieval was performed by heating slides in 10 mM sodium citrate buffer in a pressure cooker for 3 minutes to unmask epitopes. Endogenous peroxidase activity was quenched by incubation in 3% hydrogen peroxide for 10 minutes. Tissue sections were incubated overnight at 4°C with primary antibodies against DTYMK or RAF1 diluted in PBS with 1% bovine

serum albumin. HRP-conjugated secondary antibodies were applied for 30 minutes at room temperature, and signal was developed using 3,3′-diaminobenzidine chromogen for 3-5 minutes. Sections were counterstained with hematoxylin for 30 seconds to visualize nuclei and mounted with coverslips.

Cell Viability Assay (CCK-8)

Cell viability and proliferation were assessed using the Cell Counting Kit-8 (CCK-8) assay, which measures mitochondrial dehydrogenase activity as a proxy for viable cell number. Cells were plated at 3×10^3 cells per well in 96-well microtiter plates in triplicate wells per condition in complete DMEM medium. At designated time points, 10 µL of CCK-8 reagent was added to each well and cells were incubated for approximately 30 minutes at 37°C to allow color development. Absorbance at 450 nm was measured using a microplate spectrophotometer.

Transwell Chamber Assays for Cell Migration and Invasion

For the migration assay, 5×10^4 cells resuspended in 200 µL serum-free DMEM were seeded in the upper chamber of a 24-well Transwell plate with 8 µm pore polycarbonate membrane inserts. The lower chamber was filled with 600 µL DMEM supplemented with 20% FBS, which served as a chemoattractant. Cells were incubated for 24 hours at 37°C under 5% CO_2 to allow migration. Non-migratory cells remaining on the upper surface were gently removed using cotton swabs. Cells that migrated to the lower surface were fixed with 4% paraformaldehyde and stained with 0.1% crystal violet solution. For the invasion assay, the identical protocol was employed as for the migration assay, except that Transwell membranes were pre-coated with Matrigel diluted in serum-free DMEM to reconstitute basement membrane properties, and the incubation period was extended to 48 hours.

Flow Cytometry: Apoptosis Detection

At 48 hours post-treatment, cells were harvested by trypsin digestion, washed twice in ice-cold PBS, and subjected to apoptosis detection using an Annexin V-FITC/Propidium Iodide apoptosis detection kit according to the manufacturer's instructions. Cells were incubated with Annexin V-FITC and PI for 15 minutes in the dark at room temperature, and were immediately analyzed on a Cytoflex Flow Cytometer. Early apoptotic cells and late apoptotic/secondary necrotic cells were identified by gating strategies.

Intracellular ROS Measurement by fluorescence Staining

Cells were incubated with 5 µM 2′,7′-dichlorofluorescin diacetate (DCFH-DA, Sigma-Aldrich) for 30 minutes at 37°C in the dark. The non-fluorescent DCFH-

DA is passively taken up by cells and cleaved by intracellular esterases to form DCFH, which is subsequently oxidized by ROS to form highly fluorescent DCF. After incubation, cells were washed twice in PBS to remove excess dye. Fluorescence was visualized directly by immunofluorescence microscopy with 488 nm excitation, and mean fluorescence intensity was quantified.

Dual-Luciferase Reporter Assay

Wild-type and miR-7-5p seed-binding site-mutant 3′UTR fragments of both DTYMK and RAF1 were PCR-amplified from glioma cDNA using gene-specific primers containing appropriate restriction sites. The amplified fragments were directionally cloned into the psiCHECK-2 dual-luciferase reporter vector downstream of the Renilla luciferase gene. All cloned constructs were verified by Sanger DNA sequencing. HEK293T cells were co-transfected with reporter plasmid constructs together with either miR-7-5p mimic or scrambled control oligonucleotide using Lipofectamine 3000. At 48 hours post-transfection, cells were lysed and both Renilla and firefly luciferase activities were measured sequentially using the Dual-Luciferase Reporter Assay System. Renilla/firefly luciferase activity ratios were calculated for normalization.

Single-Cell RNA-Sequencing Data Analysis

Raw scRNA-seq datasets, including GSE200984 and GSE138794, were downloaded from the GEO database and processed using the Seurat R package following standard quality control and analysis workflows. QC filtering retained cells meeting the following criteria: 200-5,000 genes detected per cell and mitochondrial gene content <10% of total transcripts. Gene expression data were normalized using the NormalizeData function. Principal component analysis was performed using the top variable genes. Batch effects between different samples or studies were corrected using the Harmony batch correction algorithm. Cells were projected onto a two-dimensional UMAP space for visualization. Tumor cells were identified based on characteristic expression patterns and the presence of somatic mutations. DTYMK and mesenchymal gene signature module scores were calculated using the AddModuleScore function in Seurat.

In Vivo Xenograft Tumor Models

All animal experiments were approved by the Institutional Animal Care and Use Committee (IACUC) and conducted in strict accordance with institutional guidelines and the National Institutes of Health Guide for the Care and Use of Laboratory Animals. All measures were taken to minimize animal suffering throughout the experimental procedures.

Subcutaneous Xenograft Model. Stably transduced DTYMK-knockdown LN18 cells (sh-DTYMK; 5×10^6 cells in 200 μL PBS) or control cells (sh-control; 5×10^6 cells in 200 μL PBS) were injected subcutaneously into the bilateral flanks of 3-week-old female athymic nude mice. Tumor dimensions were measured every 7 days using digital calipers, and tumor volume was calculated according to the formula: $V = (\text{length} \times \text{width}^2) / 2$. At 6 weeks post-implantation, tumors were surgically excised, photographed, and weighed. Tumor tissues were sectioned for subsequent histopathological examination (H&E staining), Western blot analysis, and immunohistochemical detection.

Orthotopic Intracranial Implantation Model. DTYMK-knockdown GL261 cells or control cells (1×10^5 cells resuspended in 5 μL PBS) were stereotactically implanted into the right striatum of 3-week-old female C57BL/6 mice using a stereotactic frame. The injection coordinates relative to the bregma were as follows: 2.0 mm lateral to the midline (right), 0.5 mm anterior to the bregma, and 2.5 mm below the skull surface. Prior to implantation, cell lines were engineered to stably express firefly luciferase to enable non-invasive bioluminescence imaging. Tumor burden was monitored longitudinally by bioluminescence imaging using an in vivo imaging system (IVIS) following intraperitoneal injection of D-luciferin. Survival was defined as the interval from cell implantation to death. Survival curves were constructed using the Kaplan-Meier method and compared by the log-rank test.

Statistical Analysis

All statistical analyses were performed using R and GraphPad Prism software. Continuous variables are reported as mean ± standard deviation, while categorical variables are presented as frequencies and percentages. For two-group comparisons, normality of distribution was first assessed using the Shapiro-Wilk test. Normally distributed data were compared using unpaired Student's t-test, while non-normally distributed data were compared using the Mann-Whitney U test. For comparisons involving more than two groups, normally distributed data were analyzed by one-way analysis of variance with Tukey's post-hoc correction, while non-normally distributed data were analyzed using the Kruskal-Wallis test with Dunn's post-hoc correction. Overall survival in in vivo xenograft studies was assessed using Kaplan-Meier curves, with survival differences between groups evaluated using the log-rank test. Correlation analyses employed Spearman's rank correlation coefficient. Multiple statistical testing corrections were applied using the Benjamini-Hochberg false discovery rate adjustment method. All in vitro experiments were independently performed in at least three biological replicates. Statistical significance is denoted as follows: $^*P < 0.05$, $^{**}P < 0.01$, $^{***}P < 0.001$.

Results

Integration of Mitochondrial, Oxidative Stress, and Apoptosis-Related Genes Identifies DTYMK as a Key Gene in the Prognostic Risk Model

To investigate the interplay among mitochondrial dysfunction, oxidative stress, and apoptosis in glioma, we integrated three corresponding gene sets from public databases. Venn diagram analysis identified 93 consensus genes shared across all three categories (Figure 1A). Differential expression analysis using the limma package in R, comparing TCGA glioma samples with GTEx normal brain tissues, yielded 27 significantly upregulated genes ($log_2FC > 1$, $P < 0.05$; Figure 1B). Unsupervised consensus clustering of these 27 genes via ConsensusClusterPlus identified an optimal partition of $k = 2$. In both the TCGA cohort (Figure 1C-D) and the CGGA validation cohort (Figure S1A-B), patients in Cluster 2 showed significantly longer overall survival than those in Cluster 1. Heatmap analysis revealed that Cluster 1 was enriched for adverse clinicopathological features, including IDH wild-type status, 1p/19q non-deletion, MES-like subtype, higher WHO grade, MGMT promoter unmethylation, and increased mortality, whereas Cluster 2 displayed the opposite, favorable profile, as illustrated in the TCGA heatmap (Figure 1E) and the corresponding CGGA heatmap (Figure S1C).

For prognostic model construction, univariate Cox regression identified 21 candidate genes, which were further refined by LASSO and multivariate Cox regression to yield a six-gene signature comprising CASP8, DTYMK, MAPK8, PLAUR, PRODH, and TP73, with DTYMK contributing the largest coefficient, as shown in Figure 1F-H. Individual risk scores were computed from multivariate Cox coefficients and normalized expression values, and patients were stratified into high- and low-risk groups by cohort-specific median cutoffs. High-risk patients had significantly worse overall survival in the TCGA cohort (Figure 1I) and likewise in the CGGA cohort (Figure S1D). Time-dependent ROC analysis demonstrated strong discriminatory performance, with AUC values of 0.878, 0.896, and 0.867 for 1-, 3-, and 5-year survival in the TCGA cohort (Figure 1J), and AUC > 0.7 at all timepoints in the CGGA cohort (Figure S1E). Heatmap analysis of both the TCGA cohort (Figure 1K) and the CGGA cohort (Figure S1F) confirmed concordance between high-risk scores and Cluster 1 characteristics. Uni- and multivariate Cox regression analyses further established the risk score as an independent prognostic factor after adjustment for WHO grade, IDH status, 1p/19q codeletion, and MGMT methylation, as demonstrated in the TCGA cohort (Figure 1L-M) and replicated in the CGGA cohort (Figure S1G-H).

DTYMK Is Predominantly Localized to Tumor Cells, Particularly Those of the Mesenchymal Glioblastoma Subtype

Pan-cancer analysis of TCGA data revealed that DTYMK was broadly upregulated across the majority of tumor types (Figure 2A). Gene Ontology

enrichment analysis additionally indicated significant associations with epithelial-mesenchymal transition (EMT), cell cycle progression, MAPK cascade regulation, apoptosis, and oxidative stress response (Figure 2B), prompting further investigation of DTYMK in glioma. DTYMK expression increased progressively with WHO grade in both the TCGA and CGGA cohorts (Figure 2C and 2E) and was markedly elevated in the mesenchymal subtype relative to the classical, neuronal, and proneural subtypes (Figure 2D and 2F). Correlation analysis demonstrated that DTYMK expression was significantly and positively associated with MES-related and proliferation-related gene signatures in both cohorts (Figure 2G-J), collectively suggesting a role for DTYMK in driving the invasive mesenchymal phenotype.

To resolve the cellular localization of DTYMK at single-cell resolution, we analyzed two independent scRNA-seq datasets (GSE200984 and GSE138794) and found that DTYMK expression was predominantly restricted to glioma tumor cells, with substantially lower levels in tumor-associated macrophages, microglia, T cells, NK cells, B cells, and endothelial cells (Figure 2K-N). This tumor-cell-restricted expression pattern suggests that DTYMK functions as an intrinsic driver of the mesenchymal phenotype rather than a microenvironmental bystander. To further substantiate this observation, we performed integrated analysis of 11 independent single-cell datasets encompassing 93 samples (The GEO identification information is shown in Table 3). Cells were stratified by mesenchymal gene signature scores, with the top and bottom 10th percentiles designated as MES and PN groups, respectively. DTYMK expression was consistently higher in glioma cells than in other cell types (Figure 2O-P), and the DTYMK module score was significantly elevated in the MES group relative to the PN group (Figure 2Q). Overall, these single-cell analyses identify DTYMK as an intrinsic driver of the MES transcriptional program in glioma.

DTYMK Promotes Glioma Malignancy In Vitro and In Vivo

Analysis of glioma tumor tissues and adjacent normal brain tissues by Western blot and qRT-PCR revealed that DTYMK expression was significantly higher in tumor tissues compared to adjacent normal tissues. Additionally, DTYMK levels gradually increased with WHO grade (Figure 3A-B). Immunohistochemical analysis corroborated these findings, showing elevated DTYMK protein in glioma specimens (Figure 3C). Screening of eight glioma cell lines showed that DTYMK expression was substantially upregulated compared with normal astrocytes (Figure 3D-E). Based on these research results, we selected the U251 and LN18 for the subsequent functional studies. Previous reports have indicated that these two cell lines are of MES glioma cell lines [26]. To investigate the role of DTYMK in glioma, three siRNA sequences targeting DTYMK were designed, and si-DTYMK-1 demonstrated the highest knockdown

efficiency and was selected for all subsequent experiments (Figure 3F). DTYMK knockdown significantly reduced the expression of proliferation markers PCNA and Cyclin D1, downregulated the anti-apoptotic protein Bcl-2 (Figure 3G), and suppressed MES markers including CD44, ZEB1, SNAI1, and Vimentin (Figure 3H), indicating inhibition of the MES transition process. These markers are closely linked to cell cycle progression, apoptosis resistance, and MES transition in cancer cells [27]. Flow cytometry analysis revealed a marked increase in the proportion of apoptotic cells following DTYMK knockdown (Figure 3I). CCK-8 assays demonstrated that DTYMK knockdown significantly reduced cell viability in a time-dependent manner, with substantial decreases observed within 72 hours (Figure 3J-K). DCFH-DA fluorescence staining showed a significant increase in intracellular ROS levels upon DTYMK knockdown (Figure 3L), suggesting that DTYMK normally maintains ROS homeostasis within a threshold compatible with cell survival, and its depletion causes ROS accumulation exceeding the cellular antioxidant buffering capacity. This interpretation is consistent with previous studies showing that excessive ROS accumulation can damage cellular macromolecules and trigger mitochondrial apoptosis in cancer cells [28]. Transwell assays also demonstrated that DTYMK knockdown significantly impaired both the migration and invasion abilities of glioma cells (Figure 3M-N).

To validate the tumor-suppressive effects of DTYMK knockdown in vivo, two complementary xenograft models were established. Stable DTYMK-knockdown GL261 cells were implanted intracranially into mice. DTYMK knockdown significantly inhibited intracranial tumor growth (Figure 3O), and mice bearing sh-DTYMK tumors exhibited substantially prolonged survival compared to control animals (Figure 3P). Western blotting confirmed effective DTYMK downregulation in tumor tissues (Figure 3Q), and H&E staining revealed markedly restricted tumor growth in the sh-DTYMK group (Figure 3R). In a parallel experiment, stable DTYMK-knockdown LN18 cells were implanted subcutaneously in nude mice. This approach yielded consistent results: tumor volume was significantly reduced following DTYMK knockdown (Figure 3S), and DTYMK expression was substantially decreased in tumor tissues (Figure 3T). Western blotting analysis of subcutaneous tumors additionally demonstrated downregulation of MES markers following DTYMK knockdown (Figure 3U). These results demonstrate that the tumor-suppressive effects of DTYMK knockdown are consistent and reproducible both in vitro and in vivo across multiple tumor models.

DTYMK Functions as a ceRNA by Competitively Sponging miR-7-5p to Relieve Suppression of RAF1

Through bioinformatic intersection analysis of miRNAs targeting DTYMK using TargetScan and miRDB databases, six candidate miRNAs were identified, with miR-7-5p ranked as the top candidate (Figure 4A). The top three miRNAs-miR-7-5p, miR-6784-5p, and miR-5000-3p-were subsequently selected for

experimental validation. Results demonstrated that DTYMK knockdown significantly upregulated miR-7-5p expression in both U251 and LN18 cell lines (Figure 4B-C), whereas DTYMK overexpression suppressed miR-7-5p expression (Figure 4D-E). This negative regulatory relationship between DTYMK and miR-7-5p was additionally confirmed across multiple tumor types in the StarBase database, which provides experimentally supported and computationally predicted RNA-RNA interaction networks [29] (Figure 4F). Reciprocally, miR-7-5p overexpression concurrently decreased both mRNA and protein levels of DTYMK (Figure 4G-H). Gene Ontology enrichment analysis of miR-7-5p targets revealed enrichment in cell cycle regulation, cell migration, and apoptotic processes, while KEGG pathway analysis highlighted focal adhesion, MAPK signaling pathway, and glioma-related pathways (Figure 4I-J). To identify direct downstream targets of miR-7-5p, bioinformatic analysis using TargetScan and miRDB was performed, yielding seven candidate genes. Integration of these target predictions with the aforementioned enrichment results led to the selection of RAF1, a critical node in MAPK pathway regulation, for further investigation [30] (Figure 4K).

Immunohistochemical analysis confirmed high RAF1 expression in glioma tissues (Figure 4L). Consistent with miR-7-5p's regulatory role, miR-7-5p overexpression significantly reduced both mRNA and protein levels of RAF1 (Figure 4M-N). Moreover, StarBase analysis revealed a positive correlation between DTYMK and RAF1 expression across multiple tumor types (Figure 4O). Knockdown of DTYMK likewise decreased RAF1 expression (Figure 4P), further supporting a DTYMK-dependent regulatory axis. The predicted complementary binding sites between miR-7-5p and DTYMK, as well as between miR-7-5p and RAF1, are presented in Figure 4Q, with the conserved binding motif clearly depicted. To validate direct miR-7-5p-mediated repression of both targets, dual-luciferase reporter assays were performed using constructs containing wild-type miR-7-5p binding sites in DTYMK and RAF1 (Figure 4R-S), confirming sequence-specific targeting and repression of both molecules. These findings align with the ceRNA hypothesis, in which transcripts can regulate one another by competing for shared miRNAs.

DTYMK-miR-7-5p-RAF1 Axis Activates MAPK Signaling to Drive Glioma Malignancy and MES Transition

miR-7-5p overexpression phenocopied the effects of DTYMK knockdown. Specifically, miR-7-5p overexpression decreased the expression of proliferation markers PCNA and Cyclin D1 and downregulated the anti-apoptotic protein Bcl-2 (Figure 5A). In parallel, miR-7-5p overexpression suppressed MES markers CD44, ZEB1, SNAI1, and Vimentin (Figure 5B), and impaired both cell migration and invasion abilities (Figure 5C-D). CCK-8 assays revealed that miR-7-5p overexpression significantly reduced cell viability within 72 hours (Figure 5E-F). To establish RAF1 as a functionally relevant downstream

effector of the DTYMK-miR-7-5p axis, RAF1 knockdown was performed. RAF1 knockdown recapitulated all phenotypic effects observed with miR-7-5p overexpression and DTYMK knockdown. Specifically, RAF1 knockdown reduced PCNA and Cyclin D1 expression and downregulated Bcl-2 levels (Figure 5G), suppressed MES markers CD44, ZEB1, SNAI1, and Vimentin (Figure 5H), and impaired cell migration and invasion (Figure 5I-J). CCK-8 assays demonstrated that RAF1 knockdown significantly decreased cell viability within 72 hours (Figure 5K-L). These results confirm that RAF1 is a critical downstream effector mediating the functional consequences of the DTYMK-miR-7-5p regulatory axis.

To dissect the molecular mechanism in greater detail, rescue experiments were performed. miR-7-5p overexpression significantly reduced both DTYMK and RAF1 protein levels and markedly suppressed the phosphorylation of MEK and ERK, while total MEK and ERK levels remained unchanged (Figure 5M). In a complementary approach, DTYMK knockdown or overexpression resulted in concurrent alterations in RAF1, p-MEK, and p-ERK levels in a coordinated manner (Figure 5N). The RAF-MEK-ERK cascade is a canonical MAPK signaling pathway that regulates proliferation, survival, migration, and differentiation in cancer cells [31]. To confirm that MAPK pathway activation represents the primary oncogenic mechanism driving the effects of the DTYMK-miR-7-5p-RAF1 axis, DTYMK-knockdown cells were treated with epidermal growth factor (EGF) to reactivate MAPK signaling. EGF, a well-characterized activator of the MAPK pathway, can stimulate downstream responses [32]. EGF treatment substantially restored the migration and invasion abilities of DTYMK-knockdown cells and partially recovered cell viability (Figure 5O-P). In line with these observations, CCK-8 assays demonstrated that EGF significantly enhanced the proliferative capacity of DTYMK-knockdown cells (Figure 5Q-R). These findings collectively establish that MAPK pathway activation serves as the principal mechanism through which the DTYMK-miR-7-5p-RAF1 axis drives malignant progression in glioma, with particular relevance to the MES subtype transition (Figure 6).

Discussion

Mitochondrial dysfunction, oxidative stress, and apoptosis resistance are interconnected hallmarks that enable tumor cell survival and therapeutic evasion. In GBM, these processes converge to support metabolic reprogramming [33], antioxidant capacity [34], and resistance to cell death [35]. We integrated gene signatures representing these three pathways and applied LASSO regression combined with multivariate Cox regression to construct a prognostic model for glioma patients-a method suited to high-dimensional survival data [36]. The model stratified patients into high- and low-risk groups with robust performance in both training and validation cohorts. Among the six genes in the model, DTYMK carried the largest coefficient, indicating its dominant contribution to risk prediction.

Functional enrichment linked DTYMK to cell cycle progression and epithelial-mesenchymal transition (EMT), processes central to proliferation and invasion [27, 37]. DTYMK expression correlated positively with the MES gene signature and peaked in the MES subtype, implicating DTYMK in MES transition. We validated the oncogenic role of DTYMK through in vitro and in vivo experiments. DTYMK knockdown reduced proliferation markers (PCNA, Cyclin D1) [38, 39], downregulated the anti-apoptotic protein BCL-2 [40], suppressed MES markers (CD44, ZEB1, SNAI1, Vimentin) [41], and impaired migration and invasion. Moreover, after exhaustion of DTYMK, the phenomenon of cell apoptosis intensified. These phenotypes, in both the in situ intracranial transplantation model and the subcutaneous transplantation model in nude mice, were found to be able to reduce tumor burden and prolong survival time when DTYMK was knocked down, confirming its role in promoting tumor formation.

DTYMK has long been recognized as a nucleotide salvage enzyme that phosphorylates dTMP to dTDP, supplying precursors for DNA synthesis [8]. Elevated DTYMK in proliferating tumors has been attributed to increased nucleotide demand. Recent work in hepatocellular carcinoma uncovered a non-canonical function: DTYMK acts as a ceRNA, binding miR-378a-3p to sustain MAPKAPK2 expression and activate NF-κB signaling [20]. The ceRNA hypothesis, proposed in 2011, posits that transcripts sharing miRNA-binding sites compete for miRNA availability, thereby regulating each other's expression [17]. In glioma, long non-coding RNAs (e.g., LINC01426) and circular RNAs (e.g., CircXPO1) have been shown to function as ceRNAs [42, 43], but evidence for protein-coding mRNAs in this role remains limited. Through bioinformatic prediction and dual-luciferase reporter assays to confirm that the 3′UTR of DTYMK mRNA contains functional binding sites for miR-7-5p and can sequester this miRNA. miR-7 is an evolutionarily conserved miRNA family with tumor-suppressive roles [44]. miR-7 inhibits glioblastoma growth by targeting the PI3K/AKT and Raf/MEK/ERK pathways [45]. miR-7-5p, the predominant mature form, is downregulated in GBM and suppresses proliferation and invasion by targeting oncogenes including EGFR and RAF1, thereby affecting downstream PI3K/Akt signaling [46]. We identified seven miR-7-5p target genes using TargetScan and miRDB. Because both DTYMK and miR-7-5p were enriched in MAPK pathway annotations, we selected RAF1 for experimental validation. The results confirmed that DTYMK and RAF1 both bind miR-7-5p competitively.

RAF-1 belongs to the RAF family, and RAF activates the MAPK pathway [47]. RAF1 is overexpressed or aberrantly activated in many cancers and drives proliferation, survival, and metastasis [48]. Upon activation, RAF1 phosphorylates MEK1/2 and ERK1/2, promoting proliferation and MES transition [49, 50]. We found that miR-7-5p overexpression reduced glioma cell proliferation, induced apoptosis, and suppressed MES transition. miR-7-5p overexpression decreased both DTYMK and RAF1 levels and inhibited MAPK

pathway activation. Rescue experiments showed that the inhibitory effects of DTYMK knockdown could be partially reversed by adding EGF, a MAPK activator. These data support a regulatory model in which DTYMK sequesters miR-7-5p, preventing miR-7-5p-mediated repression of RAF1. Elevated RAF1 then activates MEK-ERK signaling, driving proliferation, invasion, and MES transition. Beyond its canonical role in nucleotide metabolism, DTYMK mRNA functions as a ceRNA to modulate MAPK pathway activity.

Conclusion

This study establishes DTYMK as a central regulatory factor in the progression of GBM. A six-gene prognostic model integrating mitochondrial, oxidative stress, and apoptosis-related genes was constructed and its accuracy verified in both the TCGA and CGGA cohorts. Single-cell transcriptomic analysis confirmed that DTYMK is predominantly expressed in glioma cells, especially in the MES-like subpopulation. Functional studies demonstrated that knockdown of DTYMK inhibits proliferation, migration, and invasion while inducing apoptosis. Mechanistic studies revealed that DTYMK acts as a competing endogenous RNA by sponging miR-7-5p, thereby relieving the translational inhibition of RAF1 and activating the MAPK signaling pathway to drive MES transformation, proliferation, invasion. The DTYMK-miR-7-5p-RAF1-MAPK axis, as a key oncogenic pathway, provides new strategies for targeted therapy in glioma.

Acknowledgements

The authors gratefully acknowledge the TCGA, CGGA, GEO, TargetScan, miRDB, MitoCarta, MSigDB, UCSC, and GTEx databases for providing essential data and resources for this study.

Author Contributions

Bing Zhao and ZhiHao Yang designed this study. HaoYuan Wu, ZhiWei Wang, and ZiWen Chen conducted the experiments. ZhenXing He and ChenXi Chang collected the data, while ZeJin Li, DeRan Zhang, and JinRuo Zhang performed data screening and validation. HaoYuan Wu drafted the manuscript. Bing Zhao and ZhiHao Yang revised the manuscript and supervised the entire study. All authors made substantial contributions to the work, approved the final version for submission, and declare no competing financial interests or personal relationships that could influence the reported findings. ⁺ These authors have contributed equally to this work and share first authorship.

Funding

This research was supported by grants from the Natural Science Foundation of Anhui Province (Grant Nos. 2208085MH220 and 2508085QH312) and the Anhui Medical University Foundation (Grant No. 2023xkj034).

Data Availability

The datasets generated and analyzed in this study are provided in the article and supplementary materials. Further information and inquiries can be directed to the corresponding authors.

Declarations

All participants provided informed consent in accordance with an institutional review board-approved protocol for comprehensive tumor sample analysis (Ethics Committee of the Second Affiliated Hospital of Anhui Medical University). This study adheres to the principles outlined in the Declaration of Helsinki.

Competing interests

The authors declare no competing financial interests.

Author details

Department of Neurosurgery, The Second Affiliated Hospital of Anhui Medical University, Anhui Medical University, 678 Fu Rong Road, Hefei, Anhui Province 230601, China.

References

1. Ostrom QT, Price M, Neff C, Cioffi G, Waite KA, Kruchko C, Barnholtz-Sloan JS: **CBTRUS Statistical Report: Primary Brain and Other Central Nervous System Tumors Diagnosed in the United States in 2015-2019**. *Neuro Oncol* 2022, **24**(Suppl 5):v1-v95.
2. Louis DN, Perry A, Wesseling P, Brat DJ, Cree IA, Figarella-Branger D, Hawkins C, Ng HK, Pfister SM, Reifenberger G *et al*: **The 2021 WHO Classification of Tumors of the Central Nervous System: a summary**. *Neuro Oncol* 2021, **23**(8):1231-1251.
3. Stupp R, Mason WP, van den Bent MJ, Weller M, Fisher B, Taphoorn MJ, Belanger K, Brandes AA, Marosi C, Bogdahn U *et al*: **Radiotherapy plus concomitant and adjuvant temozolomide for glioblastoma**. *N Engl J Med* 2005, **352**(10):987-996.
4. Verhaak RG, Hoadley KA, Purdom E, Wang V, Qi Y, Wilkerson MD, Miller CR, Ding L, Golub T, Mesirov JP *et al*: **Integrated genomic analysis identifies clinically relevant subtypes of glioblastoma characterized by abnormalities in PDGFRA, IDH1, EGFR, and NF1**. *Cancer Cell* 2010, **17**(1):98-110.

5. Phillips HS, Kharbanda S, Chen R, Forrest WF, Soriano RH, Wu TD, Misra A, Nigro JM, Colman H, Soroceanu L *et al*: **Molecular subclasses of high-grade glioma predict prognosis, delineate a pattern of disease progression, and resemble stages in neurogenesis**. *Cancer Cell* 2006, **9**(3):157-173.
6. Iwadate Y: **Epithelial-mesenchymal transition in glioblastoma progression**. *Oncol Lett* 2016, **11**(3):1615-1620.
7. Simon N, Friedman J, Hastie T, Tibshirani R: **Regularization Paths for Cox's Proportional Hazards Model via Coordinate Descent**. *J Stat Softw* 2011, **39**(5):1-13.
8. Su JY, Sclafani RA: **Molecular cloning and expression of the human deoxythymidylate kinase gene in yeast**. *Nucleic Acids Res* 1991, **19**(4):823-827.
9. Reichard P: **Interactions between deoxyribonucleotide and DNA synthesis**. *Annu Rev Biochem* 1988, **57**:349-374.
10. Zhang Y, Wang H, Liu Y, Yang J, Zuo X, Dong M, Zhang Z, Shi Y, Deng X, Lv Y: **Comprehensive analysis of DTYMK in pan-cancer and verification in lung adenocarcinoma**. *Biosci Rep* 2022, **42**(10).
11. Bao W, Yang H, Zhou S, Huang F, Wei Z, Peng Z: **Deoxythymidylate kinase (DTYMK) participates in cell cycle arrest to promote pancreatic adenocarcinoma progression regulated by miR-491-5p through TP53 and is associated with tumor immune infiltration**. *J Gastrointest Oncol* 2023, **14**(3):1546-1559.
12. Aloliqi AA, Farajeh AF, Al-Khader A, Kaddumi E, Eisa AA, Jaradat W: **The Impact of DTYMK as a Prognostic Marker in Colorectal Cancer**. *World J Oncol* 2023, **14**(1):84-93.
13. Yu F, Chen Y, Qiu R, Lin N, Yin Y, Zhuo Y, Lin J, Lai F: **Knockdown of deoxythymidylate kinase suppresses progression and epithelial-mesenchymal-transition of lung adenocarcinoma via STAT3 signaling**. *Physiol Genomics* 2023, **55**(5):213-221.
14. Chen X, Yuan Y, Zhou F, Huang X, Pu J, Niu X, Jiang X, Ding X: **Comprehensive analysis of DTYMK for estimating the immune microenvironment, diagnosis, prognosis effect in patients with lung adenocarcinoma**. *Aging (Albany NY)* 2022, **14**(19):7866-7876.
15. Bartel DP: **MicroRNAs: genomics, biogenesis, mechanism, and function**. *Cell* 2004, **116**(2):281-297.
16. He L, Hannon GJ: **MicroRNAs: small RNAs with a big role in gene regulation**. *Nat Rev Genet* 2004, **5**(7):522-531.
17. Salmena L, Poliseno L, Tay Y, Kats L, Pandolfi PP: **A ceRNA hypothesis: the Rosetta Stone of a hidden RNA language?** *Cell* 2011, **146**(3):353-358.
18. Tay Y, Rinn J, Pandolfi PP: **The multilayered complexity of ceRNA crosstalk and competition**. *Nature* 2014, **505**(7483):344-352.
19. Poliseno L, Salmena L, Zhang J, Carver B, Haveman WJ, Pandolfi PP: **A coding-independent function of gene and pseudogene mRNAs regulates tumour biology**. *Nature* 2010, **465**(7301):1033-1038.

20. Sun F, Liu Y, Gong T, Pan Q, Xiang T, Zhao J, Tang Y, Chen H, Han Y, Song M *et al*: **Inhibition of DTYMK significantly restrains the growth of HCC and increases sensitivity to oxaliplatin**. *Cell Death Dis* 2021, **12**(12):1093.
21. Rath S, Sharma R, Gupta R, Ast T, Chan C, Durham TJ, Goodman RP, Grabarek Z, Haas ME, Hung WHW *et al*: **MitoCarta3.0: an updated mitochondrial proteome now with sub-organelle localization and pathway annotations**. *Nucleic Acids Res* 2021, **49**(D1):D1541-D1547.
22. Liberzon A, Birger C, Thorvaldsdottir H, Ghandi M, Mesirov JP, Tamayo P: **The Molecular Signatures Database (MSigDB) hallmark gene set collection**. *Cell Syst* 2015, **1**(6):417-425.
23. Zhao Z, Zhang KN, Wang Q, Li G, Zeng F, Zhang Y, Wu F, Chai R, Wang Z, Zhang C *et al*: **Chinese Glioma Genome Atlas (CGGA): A Comprehensive Resource with Functional Genomic Data from Chinese Glioma Patients**. *Genomics Proteomics Bioinformatics* 2021, **19**(1):1-12.
24. Li H, Liang J, Wang J, Han J, Li S, Huang K, Liu C: **Mex3a promotes oncogenesis through the RAP1/MAPK signaling pathway in colorectal cancer and is inhibited by hsa-miR-6887-3p**. *Cancer Commun (Lond)* 2021, **41**(6):472-491.
25. Chen Y, Wang X: **miRDB: an online database for prediction of functional microRNA targets**. *Nucleic Acids Res* 2020, **48**(D1):D127-D131.
26. Xie H, Jiang Y, Xiang Y, Wu B, Zhao J, Huang R, Wang M, Wang Y, Liu J, Wu D *et al*: **Super-enhancer-driven LIF promotes the mesenchymal transition in glioblastoma by activating ITGB2 signaling feedback in microglia**. *Neuro Oncol* 2024, **26**(8):1438-1452.
27. Hanahan D: **Hallmarks of Cancer: New Dimensions**. *Cancer Discov* 2022, **12**(1):31-46.
28. Cai SZ, Xiong QW, Zhao LN, Ji YT, Luo ZX, Ma ZR: **beta-Elemene Triggers ROS-dependent Apoptosis in Glioblastoma Cells Through Suppressing STAT3 Signaling Pathway**. *Pathol Oncol Res* 2021, **27**:594299.
29. Li JH, Liu S, Zhou H, Qu LH, Yang JH: **starBase v2.0: decoding miRNA-ceRNA, miRNA-ncRNA and protein-RNA interaction networks from large-scale CLIP-Seq data**. *Nucleic Acids Res* 2014, **42**(Database issue):D92-97.
30. Wellbrock C, Karasarides M, Marais R: **The RAF proteins take centre stage**. *Nat Rev Mol Cell Biol* 2004, **5**(11):875-885.
31. Roberts PJ, Der CJ: **Targeting the Raf-MEK-ERK mitogen-activated protein kinase cascade for the treatment of cancer**. *Oncogene* 2007, **26**(22):3291-3310.
32. Yarden Y, Sliwkowski MX: **Untangling the ErbB signalling network**. *Nat Rev Mol Cell Biol* 2001, **2**(2):127-137.
33. Venneti S, Thompson CB: **Metabolic Reprogramming in Brain Tumors**. *Annu Rev Pathol* 2017, **12**:515-545.
34. Panieri E, Santoro MM: **ROS homeostasis and metabolism: a dangerous liason in cancer cells**. *Cell Death Dis* 2016, **7**(6):e2253.
35. Fulda S: **Cell death-based treatment of glioblastoma**. *Cell Death Dis* 2018, **9**(2):121.

36. Tibshirani R: **The Lasso Method for Variable Selection in the Cox Model**. *Statistics in Medicine* 1997, **16**(4):385-395.
37. Kalluri R, Weinberg RA: **The basics of epithelial-mesenchymal transition**. *J Clin Invest* 2009, **119**(6):1420-1428.
38. Gonzalez-Gomez P, Crecente-Campo J, Zahonero C, de la Fuente M, Hernandez-Lain A, Mira H, Sanchez-Gomez P, Garcia-Fuentes M: **Controlled release microspheres loaded with BMP7 suppress primary tumors from human glioblastoma**. *Oncotarget* 2015, **6**(13):10950-10963.
39. Qie S, Diehl JA: **Cyclin D1, cancer progression, and opportunities in cancer treatment**. *J Mol Med (Berl)* 2016, **94**(12):1313-1326.
40. Zhang Y, Ishida CT, Shu C, Kleiner G, Sanchez-Quintero MJ, Bianchetti E, Quinzii CM, Westhoff MA, Karpel-Massler G, Siegelin MD: **Inhibition of Bcl-2/Bcl-xL and c-MET causes synthetic lethality in model systems of glioblastoma**. *Sci Rep* 2018, **8**(1):7373.
41. Chen D, Li D, Xu XB, Qiu S, Luo S, Qiu E, Rong Z, Zhang J, Zheng D: **Galangin inhibits epithelial-mesenchymal transition and angiogenesis by downregulating CD44 in glioma**. *J Cancer* 2019, **10**(19):4499-4508.
42. Cao J, Tang Z, Su Z: **Long non-coding RNA LINC01426 facilitates glioblastoma progression via sponging miR-345-3p and upregulation of VAMP8**. *Cancer Cell Int* 2020, **20**:327.
43. Wang X, Wang J, An Z, Yang A, Qiu M, Tan Z: **CircXPO1 Promotes Glioblastoma Malignancy by Sponging miR-7-5p**. *Cells* 2023, **12**(6).
44. Horsham JL, Kalinowski FC, Epis MR, Ganda C, Brown RA, Leedman PJ: **Clinical Potential of microRNA-7 in Cancer**. *J Clin Med* 2015, **4**(9):1668-1687.
45. Kefas B, Godlewski J, Comeau L, Li Y, Abounader R, Hawkinson M, Lee J, Fine H, Chiocca EA, Lawler S *et al*: **microRNA-7 inhibits the epidermal growth factor receptor and the Akt pathway and is down-regulated in glioblastoma**. *Cancer Res* 2008, **68**(10):3566-3572.
46. Liu Z, Jiang Z, Huang J, Huang S, Li Y, Yu S, Yu S, Liu X: **miR-7 inhibits glioblastoma growth by simultaneously interfering with the PI3K/ATK and Raf/MEK/ERK pathways**. *Int J Oncol* 2014, **44**(5):1571-1580.
47. Lyustikman Y, Momota H, Pao W, Holland EC: **Constitutive activation of Raf-1 induces glioma formation in mice**. *Neoplasia* 2008, **10**(5):501-510.
48. Matallanas D, Birtwistle M, Romano D, Zebisch A, Rauch J, von Kriegsheim A, Kolch W: **Raf family kinases: old dogs have learned new tricks**. *Genes Cancer* 2011, **2**(3):232-260.
49. Cseh B, Doma E, Baccarini M: **"RAF" neighborhood: protein-protein interaction in the Raf/Mek/Erk pathway**. *FEBS Lett* 2014, **588**(15):2398-2406.
50. Olea-Flores M, Zuniga-Eulogio MD, Mendoza-Catalan MA, Rodriguez-Ruiz HA, Castaneda-Saucedo E, Ortuno-Pineda C, Padilla-Benavides T, Navarro-Tito N: **Extracellular-Signal Regulated Kinase: A Central Molecule Driving Epithelial-Mesenchymal Transition in Cancer**. *Int J Mol Sci* 2019, **20**(12).

FIGURE LEGENDS

Figure 1 | Integrated Mitochondria-Oxidative Stress-Apoptosis Prognostic Signature Identifies DTYMK as Dominant Risk Gene, Validated in TCGA Training Cohort

A Three-way Venn diagram of mitochondria-related (n = 2004), oxidative stress-related (n = 1373), and apoptosis-related (n = 581) genes; 93 consensus genes identified at intersection. **B** Differential expression analysis in TCGA glioma (n = 667) vs GTEx normal brain (n = 1124) identified 27 upregulated genes ($log_2FC > 1$, $P < 0.05$). **C** Consensus clustering CDF curves with k = 2 as optimal. **D** Kaplan-Meier survival analysis by cluster in TCGA cohort. **E** Cluster 1 significantly enriched in adverse features including high WHO grade, IDH wild-type, LGm6/LGr4 subtypes, non-codeleted 1p/19q, MES subtype, and unmethylated MGMT. **F** Univariate Cox regression identifying 21 candidate genes. **G-H** LASSO and multivariate Cox regression jointly identified six genes, with DTYMK showing the greatest contribution. **I** Kaplan-Meier survival analysis showing significantly lower overall survival in high-risk vs low-risk groups. **J** ROC curves at 1/3/5 years (AUC = 0.878/0.896/0.867). **K** High-risk group significantly enriched in the same adverse features as Cluster 1. **L-M** Univariate and multivariate Cox regression analyses confirmed WHO grade and risk score as independent prognostic factors.

Figure 2 | DTYMK Is Predominantly Localized to Tumor Cells, Particularly Those of the Mesenchymal Glioblastoma Subtype

A Pan-cancer analysis revealed elevated DTYMK expression across multiple tumor types. **B** GO enrichment analysis showed enrichment in EMT, cell cycle, MAPK signaling, apoptosis, and oxidative stress. **C-D** In TCGA, DTYMK expression gradually increased with WHO grade, with highest expression in MES subtype. **E-F** In CGGA, DTYMK expression similarly increased with WHO grade, with highest expression in MES subtype. **G-H** In TCGA, Spearman correlation analysis showed strong positive correlations between DTYMK and both mesenchymal-related and proliferation-related genes. **I-J** In CGGA, similar strong positive correlations were observed. **K-N** Single-cell RNA sequencing analysis (GSE200984, GSE138794) revealed that DTYMK expression was predominantly localized to tumor cells. **O-Q** Integrated analysis of 11 datasets showed DTYMK expression primarily in tumor cells, with significantly higher values in MES vs PN subgroup.

Figure 3 | DTYMK Knockdown Suppresses Proliferation, Promotes Apoptosis and ROS, Inhibits Mesenchymal Transition In Vitro and In Vivo

A qRT-PCR results showed elevated DTYMK expression in tumor tissues compared to normal tissues, increasing with WHO grade. **B** Western blot analysis confirmed elevated DTYMK protein in tumor tissues. **C** Immunohistochemistry showed significantly increased DTYMK expression in

gliomas. **D-E** DTYMK expression was higher in glioma cell lines (U251, LN18) than in astrocytes. **F** si-DTYMK-1 achieved the highest knockdown efficiency. **G** DTYMK knockdown reduced proliferation (PCNA, Cyclin D1) and anti-apoptotic markers (Bcl-2). **H** DTYMK knockdown reduced MES markers (CD44, ZEB1, SNAI1, Vimentin). **I** Flow cytometry showed increased proportion of apoptotic cells. **J-K** CCK-8 assays showed gradual cell survival decrease over time. **L** DTYMK knockdown elevated reactive oxygen species levels in glioma cells. **M-N** Transwell assays revealed impaired migration and invasion abilities following DTYMK knockdown. **O-Q** Orthotopic intracranial tumor models demonstrated that DTYMK knockdown inhibited tumor growth, prolonged survival, and reduced tumor tissue DTYMK expression. **R** H&E staining showed reduced tumor cell density in sh-DTYMK lesion areas. **S-T** Subcutaneous xenograft models showed that DTYMK knockdown inhibited tumor growth and volume while reducing tumor tissue DTYMK expression. **U** Continuous DTYMK downregulation in subcutaneous tumors inhibited MES marker expression.

Figure 4 | DTYMK Functions as ceRNA Sponging miR-7-5p to Relieve RAF1 Suppression

A Cross-analysis of TargetScan and miRDB databases identified miR-7-5p, miR-6784-5p, and miR-5000-3p as candidate target miRNAs. **B-C** qRT-PCR results showed that DTYMK knockdown upregulated miR-7-5p expression. **D-E** DTYMK overexpression inhibited miR-7-5p expression. **F** StarBase database revealed negative correlation between DTYMK and miR-7-5p across multiple tumors. **G-H** miR-7-5p overexpression decreased both DTYMK mRNA and protein levels. **I-J** GO and KEGG enrichment analyses of miR-7-5p targets showed enrichment in cell cycle, migration, apoptosis, focal adhesion, MAPK signaling pathway, and glioma. **K** Cross-analysis of TargetScan and miRDB databases identified RAF1 as candidate target gene. **L** Immunohistochemistry showed significantly elevated RAF1 expression in gliomas. **M-N** miR-7-5p overexpression decreased both RAF1 mRNA and protein levels. **O** StarBase database indicated positive correlation between DTYMK and RAF1 across multiple tumor types. **P** Western blot showed DTYMK knockdown decreased RAF1. **Q** Sequence alignment revealed conserved miR-7-5p binding sites in DTYMK and RAF1 3'UTRs. **R-S** Dual-luciferase assays showed that miR-7-5p inhibited gene expression of wild-type DTYMK and RAF1.

Figure 5 | DTYMK-miR-7-5p-RAF1 Axis Activates MAPK Signaling

A miR-7-5p overexpression reduced proliferation (PCNA, Cyclin D1) and anti-apoptotic markers (Bcl-2). **B** miR-7-5p overexpression reduced MES markers (CD44, ZEB1, SNAI1, Vimentin). **C-D** Transwell assays demonstrated that miR-7-5p overexpression inhibited both migration and invasion abilities. **E-F** CCK-8 assays showed that miR-7-5p overexpression gradually decreased cell survival rate over time. **G** RAF1 knockdown reduced proliferation (PCNA, Cyclin D1)

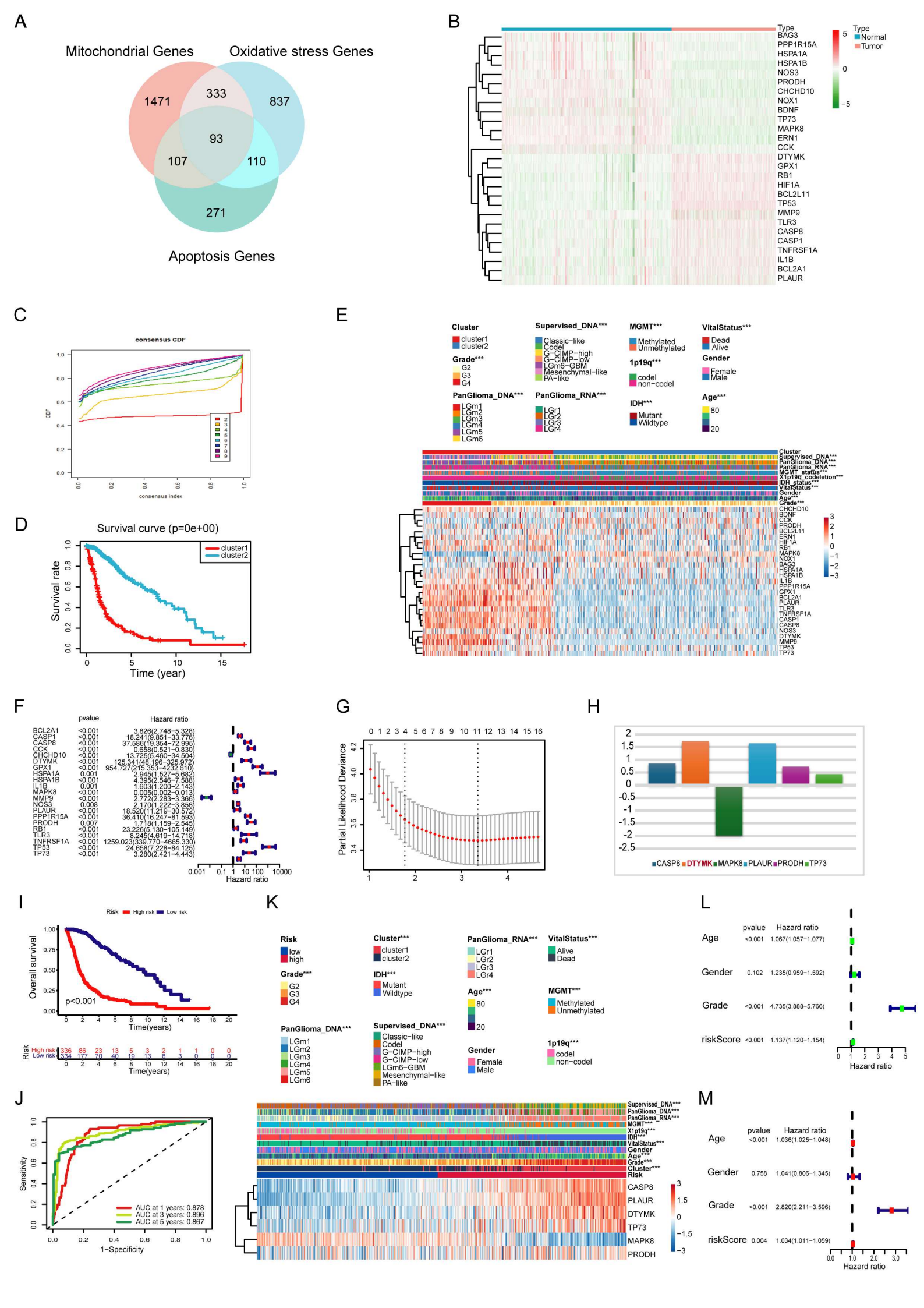
and anti-apoptotic markers (Bcl-2). **H** RAF1 knockdown reduced MES markers (CD44, ZEB1, SNAI1, Vimentin). **I-J** Transwell assays showed that RAF1 knockdown inhibited both migration and invasion abilities. **K-L** CCK-8 assays showed that RAF1 knockdown gradually decreased cell survival rate over time. **M** miR-7-5p overexpression decreased DTYMK, RAF1, p-MEK, and p-ERK expression. **N** DTYMK knockdown decreased RAF1, p-MEK, and p-ERK expression; overexpressing DTYMK rescued these effects. **O-P** DTYMK knockdown impaired migration and invasion; adding EGF rescued these defects. **Q-R** DTYMK knockdown inhibited cell viability; adding EGF rescued this effect.

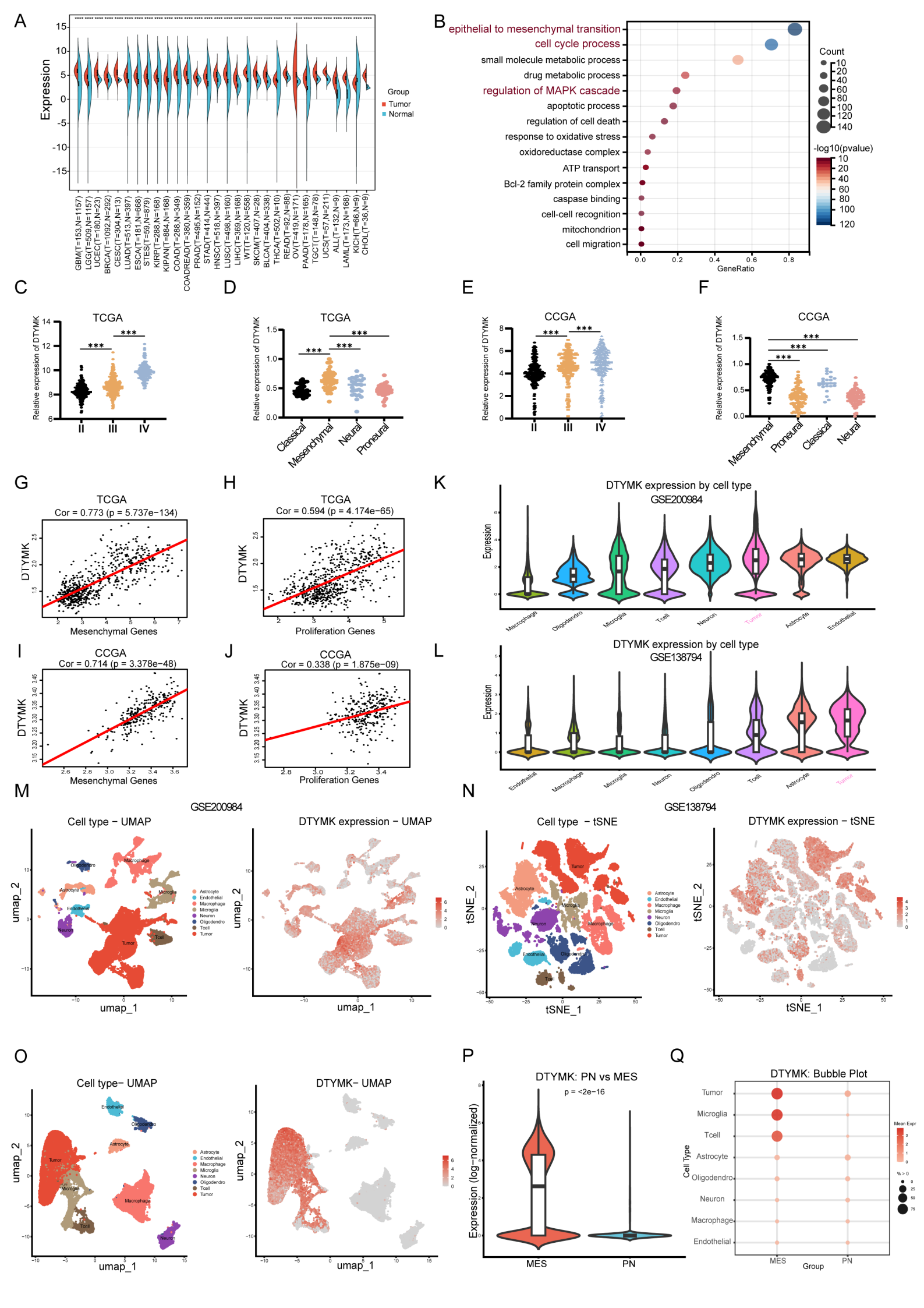
Figure 6 | Graphical Abstract

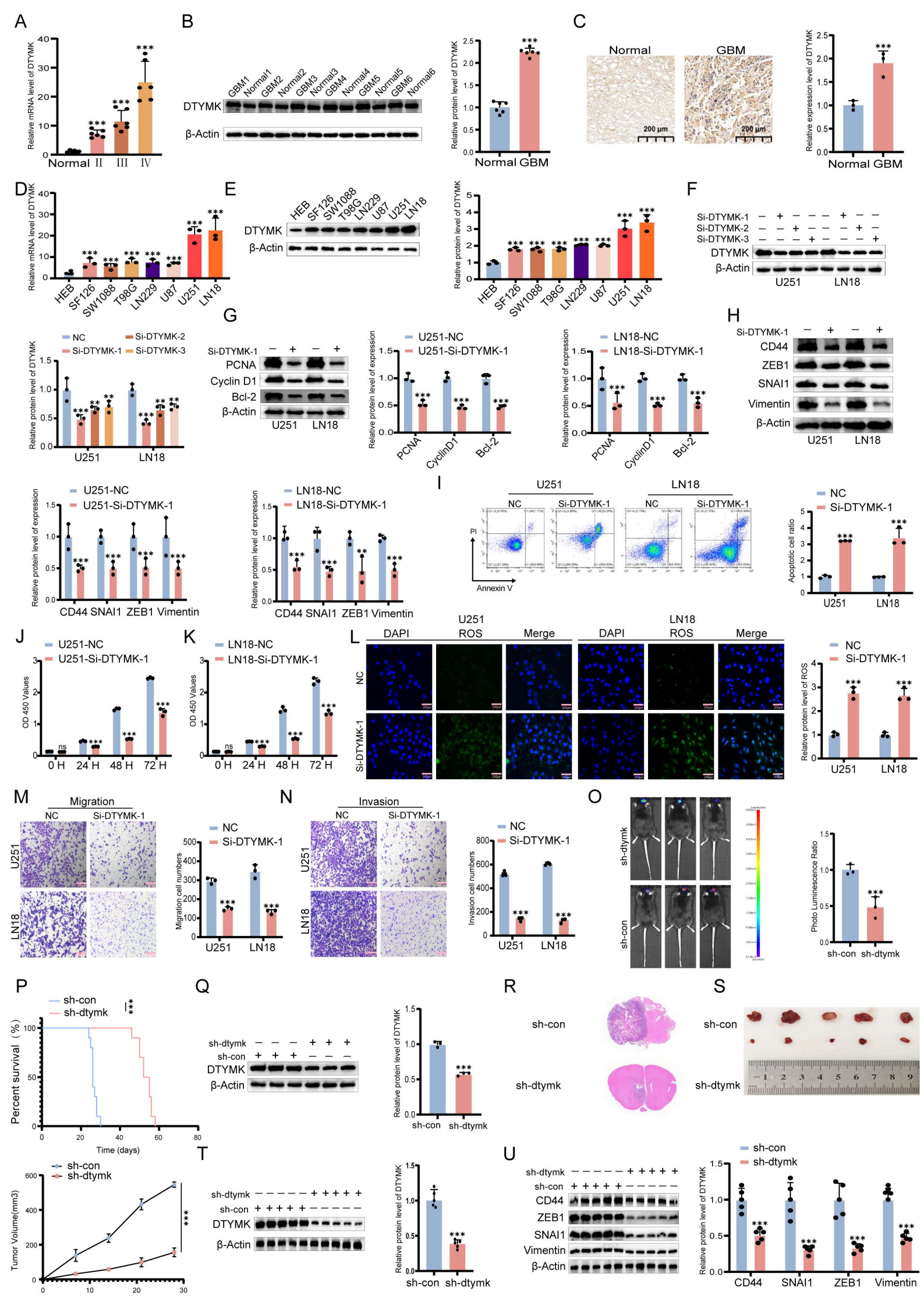
These findings collectively establish that MAPK pathway activation serves as the principal mechanism through which the DTYMK-miR-7-5p-RAF1 axis drives malignant progression in glioma, with particular relevance to the MES subtype transition

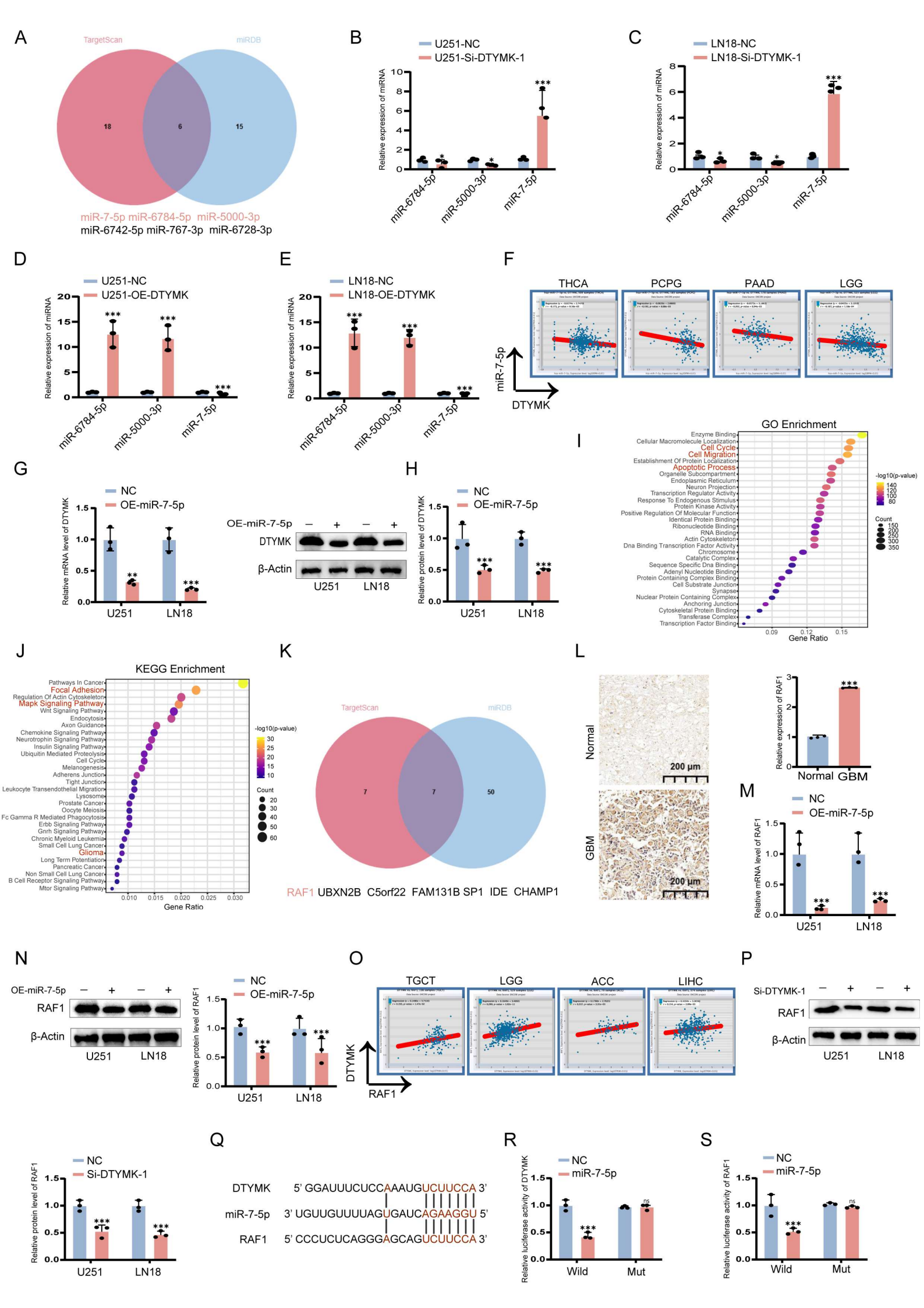
Figure S1 | CGGA Validation Cohort

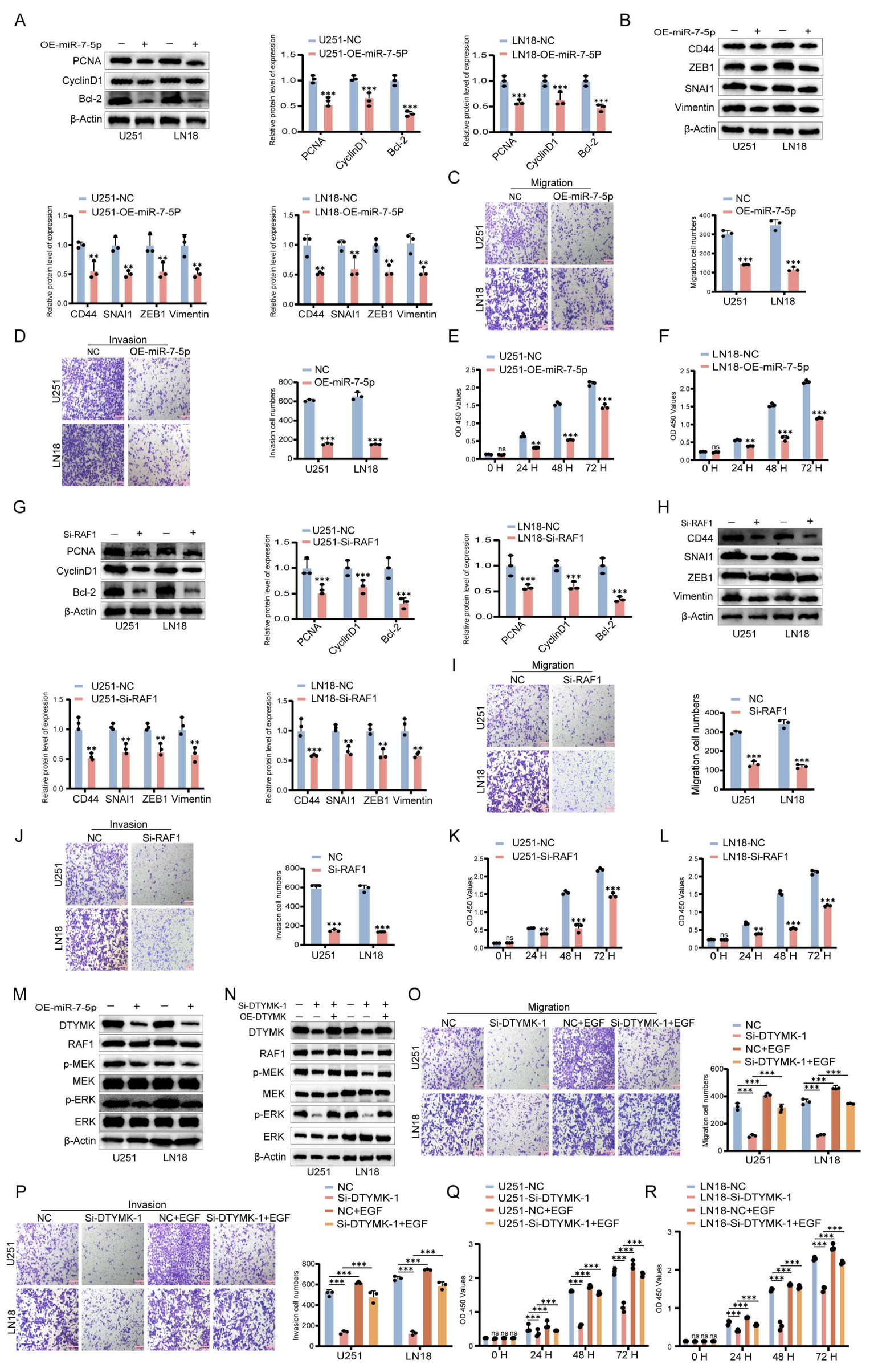
A Consensus clustering CDF curves with k = 2 as optimal. **B** Kaplan-Meier survival analysis by cluster. **C** Cluster 1 significantly enriched in adverse features including high WHO grade, IDH wild-type, non-codeleted 1p/19q, and unmethylated MGMT. **D** Kaplan-Meier survival analysis showing significantly lower overall survival in high-risk vs low-risk groups. **E** ROC curves at 1/3/5 years (AUC = 0.704/0.738/0.730). **F** High-risk group significantly enriched in the same adverse features as Cluster 1. **G-H** Univariate and multivariate Cox regression analyses confirmed that WHO grade and risk score serve as independent prognostic factors.

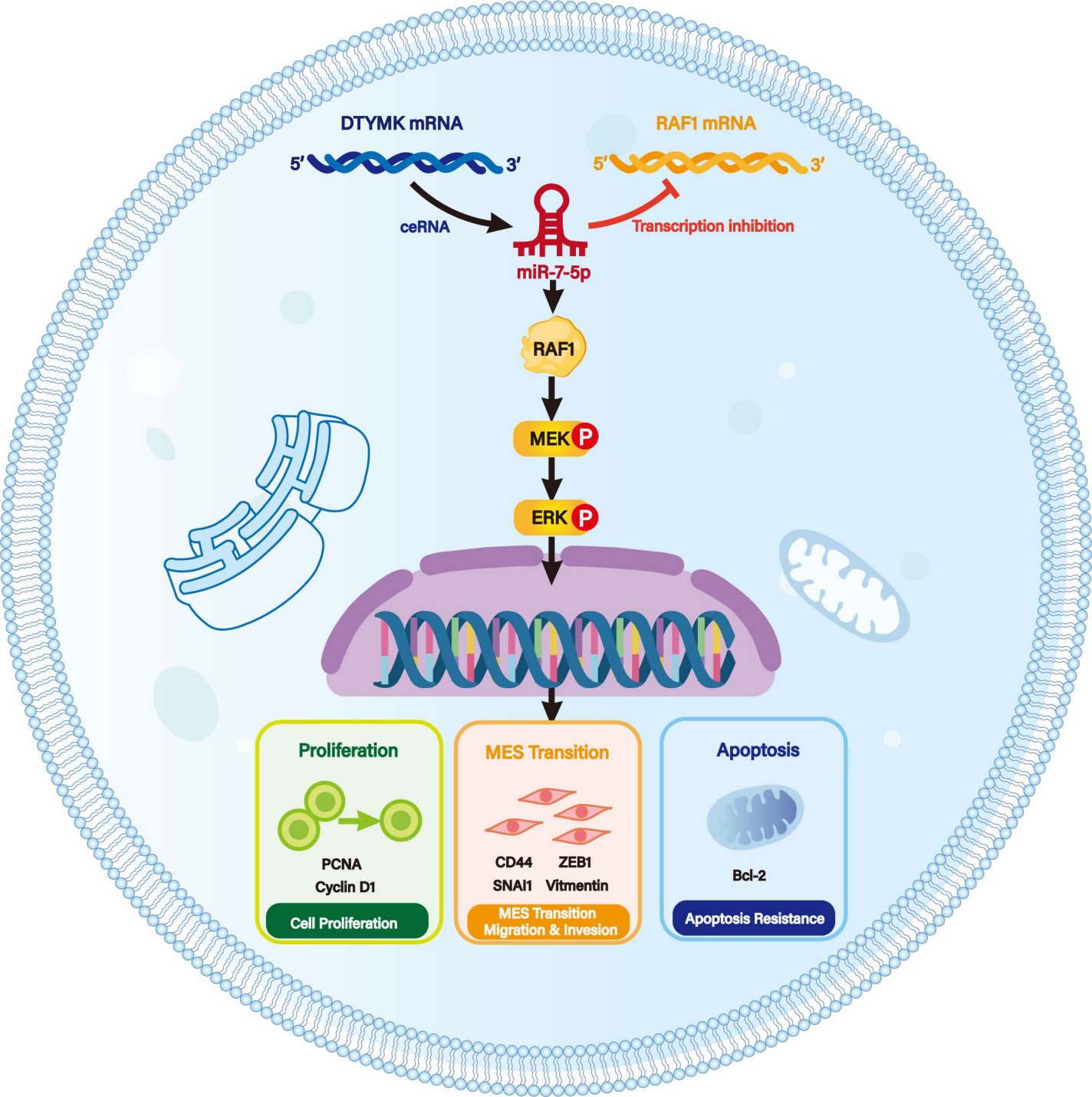

A
Mitochondrial Genes
Oxidative stress Genes
Apoptosis Genes
1471
333
837
93
107
110
271
B
Type
Normal
Tumor
BAG3
PPP1R15A
HSPA1A
HSPA1B
NOS3
PRODH
CHCHD10
NOX1
BDNF
TP73
MAPK8
ERN1
CCK
DTYMK
GPX1
RB1
HIF1A
BCL2L11
TP53
MMP9
TLR3
CASP8
CASP1
TNFRSF1A
IL1B
BCL2A1
PLAUR
C
consensus CDF
CDF
consensus index
D
Survival curve (p=0e+00)
cluster1
cluster2
Survival rate
Time (year)
E
Cluster
cluster1
cluster2
Grade***
G2
G3
G4
PanGlioma_DNA***
LGm1
LGm2
LGm3
LGm4
LGm5
LGm6
Supervised_DNA***
Classic-like
Codel
G-CIMP-high
G-CIMP-low
LGm6-GBM
Mesenchymal-like
PA-like
PanGlioma_RNA***
LGr1
LGr2
LGr3
LGr4
MGMT***
Methylated
Unmethylated
1p19q***
codel
non-codel
IDH***
Mutant
Wildtype
VitalStatus***
Dead
Alive
Gender
Female
Male
Age***
80
20
F
pvalue
Hazard ratio
BCL2A1 <0.001 3.826(2.748−5.328)
CASP1 <0.001 18.241(9.851−33.776)
CASP8 <0.001 37.586(19.354−72.995)
CCK <0.001 0.658(0.521−0.830)
CHCHD10 <0.001 13.725(5.460−34.504)
DTYMK <0.001 125.341(48.196−325.972)
GPX1 <0.001 954.727(215.353−4232.610)
HSPA1A 0.001 2.945(1.527−5.682)
HSPA1B <0.001 4.395(2.546−7.588)
IL1B 0.001 1.603(1.200−2.143)
MAPK8 <0.001 0.005(0.002−0.013)
MMP9 <0.001 2.772(2.283−3.366)
NOS3 0.008 2.170(1.222−3.856)
PLAUR <0.001 18.520(11.219−30.572)
PPP1R15A <0.001 36.410(16.247−81.593)
PRODH 0.007 1.718(1.159−2.545)
RB1 <0.001 23.226(5.130−105.149)
TLR3 <0.001 8.245(4.619−14.718)
TNFRSF1A <0.001 1259.023(339.770−4665.330)
TP53 <0.001 24.658(7.228−84.125)
TP73 <0.001 3.280(2.421−4.443)
Hazard ratio
G
Partial Likelihood Deviance
H
CASP8
DTYMK
MAPK8
PLAUR
PRODH
TP73
I
Risk
High risk
Low risk
Overall survival
p<0.001
Time(years)
High risk 336 86 23 13 5 3 2 1 1 0 0
Low risk 334 177 70 40 19 13 6 3 0 0 0
K
Risk
low
high
Grade***
G2
G3
G4
PanGlioma_DNA***
LGm1
LGm2
LGm3
LGm4
LGm5
LGm6
Cluster***
cluster1
cluster2
IDH***
Mutant
Wildtype
Supervised_DNA***
Classic-like
Codel
G-CIMP-high
G-CIMP-low
LGm6-GBM
Mesenchymal-like
PA-like
PanGlioma_RNA***
LGr1
LGr2
LGr3
LGr4
Age***
80
20
Gender
Female
Male
VitalStatus***
Alive
Dead
MGMT***
Methylated
Unmethylated
1p19q***
codel
non-codel
L
pvalue
Hazard ratio
Age <0.001 1.067(1.057−1.077)
Gender 0.102 1.235(0.959−1.592)
Grade <0.001 4.735(3.888−5.766)
riskScore <0.001 1.137(1.120−1.154)
Hazard ratio
J
Sensitivity
1−Specificity
AUC at 1 years: 0.878
AUC at 3 years: 0.896
AUC at 5 years: 0.867
Supervised_DNA***
PanGlioma_DNA***
PanGlioma_RNA***
MGMT***
X1p19q***
IDH***
VitalStatus***
Gender
Age***
Grade***
Cluster***
Risk
CASP8
PLAUR
DTYMK
TP73
MAPK8
PRODH
M
pvalue
Hazard ratio
Age <0.001 1.036(1.025−1.048)
Gender 0.758 1.041(0.806−1.345)
Grade <0.001 2.820(2.211−3.596)
riskScore 0.004 1.034(1.011−1.059)
Hazard ratio


A
Expression
Group
Tumor
Normal
GBM(T=153,N=1157)
LGG(T=509,N=1157)
UCEC(T=180,N=23)
BRCA(T=1092,N=292)
CESC(T=304,N=13)
LUAD(T=513,N=397)
ESCA(T=181,N=668)
STES(T=59,N=879)
KIRP(T=288,N=168)
KIPAN(T=884,N=168)
COAD(T=288,N=349)
COADREAD(T=380,N=359)
PRAD(T=495,N=152)
STAD(T=414,N=44)
HNSC(T=518,N=397)
LUSC(T=498,N=160)
LIHC(T=369,N=168)
WT(T=120,N=558)
SKCM(T=407,N=28)
BLCA(T=404,N=338)
THCA(T=502,N=10)
READ(T=92,N=88)
OV(T=419,N=171)
PAAD(T=178,N=165)
TGCT(T=148,N=78)
UCS(T=57,N=211)
ALL(T=132,N=9)
LAML(T=173,N=168)
KICH(T=66,N=9)
CHOL(T=36,N=9)
B
epithelial to mesenchymal transition
cell cycle process
small molecule metabolic process
drug metabolic process
regulation of MAPK cascade
apoptotic process
regulation of cell death
response to oxidative stress
oxidoreductase complex
ATP transport
Bcl-2 family protein complex
caspase binding
cell-cell recognition
mitochondrion
cell migration
GeneRatio
Count
-log10(pvalue)
C
TCGA
Relative expression of DTYMK
II
III
IV
D
TCGA
Classical
Mesenchymal
Neural
Proneural
E
CCGA
F
CCGA
Mesenchymal
Proneural
Classical
Neural
G
TCGA
Cor = 0.773 (p = 5.737e−134)
DTYMK
Mesenchymal Genes
H
TCGA
Cor = 0.594 (p = 4.174e−65)
Proliferation Genes
K
DTYMK expression by cell type
GSE200984
Expression
Macrophage
Oligodendro
Microglia
Tcell
Neuron
Tumor
Astrocyte
Endothelial
I
CCGA
Cor = 0.714 (p = 3.378e−48)
J
CCGA
Cor = 0.338 (p = 1.875e−09)
L
DTYMK expression by cell type
GSE138794
M
GSE200984
Cell type − UMAP
DTYMK expression − UMAP
umap_1
umap_2
N
GSE138794
Cell type − tSNE
DTYMK expression − tSNE
tSNE_1
tSNE_2
O
Cell type− UMAP
DTYMK− UMAP
P
DTYMK: PN vs MES
p = <2e−16
Expression (log−normalized)
MES
PN
Q
DTYMK: Bubble Plot
Cell Type
Group
Mean Expr
% > 0


A
Relative mRNA level of DTYMK
Normal II III IV
B
GBM1 Normal1 GBM2 Normal2 GBM3 Normal3 GBM4 Normal4 GBM5 Normal5 GBM6 Normal6
DTYMK
β-Actin
Relative protein level of DTYMK
Normal GBM
C
Normal
GBM
200 μm
Relative expression level of DTYMK
Normal GBM
D
Relative mRNA level of DTYMK
HEB SF126 SW1088 T98G LN229 U87 U251 LN18
E
HEB SF126 SW1088 T98G LN229 U87 U251 LN18
DTYMK
β-Actin
Relative protein level of DTYMK
F
Si-DTYMK-1
Si-DTYMK-2
Si-DTYMK-3
DTYMK
β-Actin
U251 LN18
G
NC
Si-DTYMK-1
Si-DTYMK-2
Si-DTYMK-3
Relative protein level of DTYMK
U251 LN18
PCNA
Cyclin D1
Bcl-2
β-Actin
U251-NC
U251-Si-DTYMK-1
Relative protein level of expression
PCNA CyclinD1 Bcl-2
LN18-NC
LN18-Si-DTYMK-1
H
Si-DTYMK-1
CD44
ZEB1
SNAI1
Vimentin
β-Actin
U251 LN18
I
U251
LN18
NC
Si-DTYMK-1
PI
Annexin V
Apoptotic cell ratio
U251 LN18
J
U251-NC
U251-Si-DTYMK-1
OD 450 Values
0 H 24 H 48 H 72 H
K
LN18-NC
LN18-Si-DTYMK-1
L
DAPI
ROS
Merge
NC
Si-DTYMK-1
Relative protein level of ROS
M
Migration
NC
Si-DTYMK-1
U251
LN18
Migration cell numbers
N
Invasion
Invasion cell numbers
O
sh-dtymk
sh-con
Photo Luminescence Ratio
P
sh-con
sh-dtymk
Percent survival (%)
Time (days)
Tumor Volume(mm3)
Q
sh-dtymk
sh-con
DTYMK
β-Actin
Relative protein level of DTYMK
R
S
T
U
CD44
ZEB1
SNAI1
Vimentin
β-Actin
Relative protein level of DTYMK


A
TargetScan
miRDB
18
6
15
miR-7-5p miR-6784-5p miR-5000-3p
miR-6742-5p miR-767-3p miR-6728-3p
B
U251-NC
U251-Si-DTYMK-1
Relative expression of miRNA
miR-6784-5p
miR-5000-3p
miR-7-5p
C
LN18-NC
LN18-Si-DTYMK-1
D
U251-NC
U251-OE-DTYMK
E
LN18-NC
LN18-OE-DTYMK
F
THCA
PCPG
PAAD
LGG
miR-7-5p
DTYMK
G
NC
OE-miR-7-5p
Relative mRNA level of DTYMK
U251
LN18
OE-miR-7-5p
DTYMK
β-Actin
H
Relative protein level of DTYMK
I
GO Enrichment
Enzyme Binding
Cellular Macromolecule Localization
Cell Cycle
Cell Migration
Establishment Of Protein Localization
Apoptotic Process
Organelle Subcompartment
Endoplasmic Reticulum
Neuron Projection
Transcription Regulator Activity
Response To Endogenous Stimulus
Protein Kinase Activity
Positive Regulation Of Molecular Function
Identical Protein Binding
Ribonucleotide Binding
RNA Binding
Actin Cytoskeleton
Dna Binding Transcription Factor Activity
Chromosome
Catalytic Complex
Sequence Specific Dna Binding
Adenyl Nucleotide Binding
Protein Containing Complex Binding
Cell Substrate Junction
Synapse
Nuclear Protein Containing Complex
Anchoring Junction
Cytoskeletal Protein Binding
Transferase Complex
Transcription Factor Binding
-log10(p-value)
Count
Gene Ratio
J
KEGG Enrichment
Pathways In Cancer
Focal Adhesion
Regulation Of Actin Cytoskeleton
Mapk Signaling Pathway
Wnt Signaling Pathway
Endocytosis
Axon Guidance
Chemokine Signaling Pathway
Neurotrophin Signaling Pathway
Insulin Signaling Pathway
Ubiquitin Mediated Proteolysis
Cell Cycle
Melanogenesis
Adherens Junction
Tight Junction
Leukocyte Transendothelial Migration
Lysosome
Prostate Cancer
Oocyte Meiosis
Fc Gamma R Mediated Phagocytosis
Erbb Signaling Pathway
Gnrh Signaling Pathway
Chronic Myeloid Leukemia
Small Cell Lung Cancer
Glioma
Long Term Potentiation
Pancreatic Cancer
Non Small Cell Lung Cancer
B Cell Receptor Signaling Pathway
Mtor Signaling Pathway
-log10(p-value)
Count
Gene Ratio
K
TargetScan
miRDB
7
7
50
RAF1 UBXN2B C5orf22 FAM131B SP1 IDE CHAMP1
L
Normal
GBM
200 μm
Relative expression of RAF1
Normal
GBM
M
NC
OE-miR-7-5p
Relative mRNA level of RAF1
U251
LN18
N
OE-miR-7-5p
RAF1
β-Actin
U251
LN18
NC
OE-miR-7-5p
Relative protein level of RAF1
O
TGCT
LGG
ACC
LIHC
DTYMK
RAF1
P
Si-DTYMK-1
RAF1
β-Actin
U251
LN18
NC
Si-DTYMK-1
Relative protein level of RAF1
Q
DTYMK 5' GGAUUUCUCCAAAUGUCUUCCA 3'
miR-7-5p 3' UGUUGUUUUAGUGAUCAGAAGGU 5'
RAF1 5' CCCUCUCAGGGAGCAGUCUUCCA 3'
R
NC
miR-7-5p
Relative luciferase activity of DTYMK
Wild
Mut
ns
S
NC
miR-7-5p
Relative luciferase activity of RAF1
Wild
Mut
ns


A
OE-miR-7-5p
PCNA
CyclinD1
Bcl-2
β-Actin
U251
LN18
U251-NC
U251-OE-miR-7-5P
LN18-NC
LN18-OE-miR-7-5P
Relative protein level of expression
B
CD44
ZEB1
SNAI1
Vimentin
C
Migration
NC
OE-miR-7-5p
Migration cell numbers
D
Invasion
Invasion cell numbers
E
OD 450 Values
0 H
24 H
48 H
72 H
F
G
Si-RAF1
U251-Si-RAF1
LN18-Si-RAF1
H
I
J
K
L
M
DTYMK
RAF1
p-MEK
MEK
p-ERK
ERK
N
Si-DTYMK-1
OE-DTYMK
O
NC+EGF
Si-DTYMK-1+EGF
P
Q
U251-Si-DTYMK-1
U251-NC+EGF
U251-Si-DTYMK-1+EGF
R
LN18-Si-DTYMK-1
LN18-NC+EGF
LN18-Si-DTYMK-1+EGF


DTYMK mRNA
5′
3′
RAF1 mRNA
5′
3′
ceRNA
Transcription inhibition
miR-7-5p
RAF1
MEK P
ERK P
Proliferation
PCNA
Cyclin D1
Cell Proliferation
MES Transition
CD44
ZEB1
SNAI1
Vitmentin
MES Transition
Migration & Invesion
Apoptosis
Bcl-2
Apoptosis Resistance

Supplementary Files

This is a list of supplementary files associated with this preprint. Click to download.

- Table1.xlsx
- Table2.xlsx
- Table3.xlsx
- FigureS1.tif